Composites Part B 177 (2019) 107379

Contents lists available at ScienceDirect

Composites Part B

journal homepage: www.elsevier.com/locate/compositesb

Effects of ozonized carbon black on fracture and post-cracking toughness of carbon fiber-reinforced epoxy composites

Seong Hwang Kim [a], Sang Jin Park [a], Kyong Yop Rhee [b,**], Soo-Jin Park [a,*]

[a] Department of Chemistry, Inha University, 100 Inharo, Incheon, 22212, South Korea
[b] Department of Mechanical Engineering, College of Engineering, Kyung Hee University, Yongin, 17104, South Korea

ARTICLE INFO

Keywords:
Polymer-matrix composites (PMCs)
Physical properties
Surface properties
Fracture toughness

ABSTRACT

Improving the fracture and post-cracking toughness of carbon fiber-reinforced composites based on thermosetting epoxy matrices are of significant interest in a wide range of applications. Herein, we report the synergistic integration of multi-scale composites by combining nano-scale filler and macro-scale fiber reinforcement inspired by the hierarchy approach. For the nano-scale filler, the carbon black (CB) surface was successfully modified using ozone treatment and thereby achieved highly efficient dispersion and interfacial properties. The reinforcing mechanisms were also analyzed, and the improvements on dispersion and interfacial properties should mainly be attributed to mechanical interlocking effect. For all of the multi-scale composites fabricated, the ozone-functionalized CB content was found to be optimal at 5 wt%, which improved the fracture and post-cracking toughness by 12.5% and 61.9%, respectively, compared with pristine CB.

1. Introduction

In recent decades, carbon fiber-reinforced polymer composites (CFRPs) have been used extensively in the aerospace and automobile industries because of their high stiffness, excellent tensile strength, low weight, and high thermal stability [1–4]. However, a long-standing problem with epoxy resins widely used in engineering structures as a matrix phase in CFRPs is their relatively low fracture toughness, which results in poor resistance to crack propagation [5–7]. Many strategies have been developed to overcome this problem and one of the most popular is a multi-scale structure, which is a promising chemical approach that provides superior performance in synergistically integrated nano-scale materials and macro-scale fibers in composite applications. Recent researches by many professionals have reported that incorporating carbon nanotubes [8,9], cellulose [10], nano-silica [11,12], graphene, and graphene oxide [13–15] into epoxy matrix can enhance the fracture toughness. Thus, enhancing the hierarchy structure between carbon fibers (CFs) and the epoxy matrix with various nano-scale fillers is critical.

It has been demonstrated that carbon black (CB) is an ideal candidate for the selective reinforcement of CF-epoxy matrix interfacial regions owing to its outstanding thermal, electrical, and mechanical performance [16–19]. It as a kind of carbon material that has a microcrystalline structure with carbon atoms forming hexagonal planes in a manner similar to graphite [20,21]. The hexagonal planes are basal and prismatic, with prismatic having higher activity than basal, which means that functional groups can be easily generated at edge sites. However, there is a lot of van der Waals force between CB particles, thus leading to very strong interactions. Thus, the scope of CB application in practical devices has been largely hampered by their poor dispersion within the polymer resin and to address this problem, much effort has been made to enhance the workability of CB. Several recent studies have verified that surface functionalization [22,23] and use of a variety of dispersing agents [24–27] were developed to overcome these challenges.

As is well known, plasma treatment and high concentration acid has shown promising results to attach oxygen groups onto nano-scale material surfaces. However, it has been reported that damage/defects are unavoidably introduced onto the nano-scale material surfaces when exposing nano-scale materials to plasma irradiation [28]. In addition, the acid treatment requires strong acids or harmful chemical substances and generally results in low yield, and consequently, the nano-scale materials contain traces of undesirable chemicals and thus require further refining [29]. For dispersing agents, to prepare multi-scale

* Corresponding author.
** Corresponding author.
E-mail addresses: rheeky@khu.ac.kr (K.Y. Rhee), sjpark@inha.ac.kr (S.-J. Park).

https://doi.org/10.1016/j.compositesb.2019.107379
Received 28 May 2019; Received in revised form 9 August 2019; Accepted 24 August 2019
Available online 27 August 2019

composites with a homogenous dispersion of CB, the epoxy matrixes are requested to be water-soluble or emulsible. In other words, even though CBs can be dispersed in water at the aid of surfactants or copolymer, it is still difficult to uniformly disperse CBs within the epoxy matrix. Although these different methods have demonstrated to be efficacious, they still have some demerits when applied in pragmatic applications.

Ozone surface treatment is considered to be an effective method because it can easily provide ozone-rich single oxygen radicals in an oxidizing atmosphere without incurring structural damage [30–32]. In addition, modifying nanofillers with ozone is a relatively easy, low cost, and highly efficient method [33]. Arnault et al. [34] modified the surface of nanodiamonds using ozone and revealed a higher oxygen concentration at the nanodiamond surfaces with abundant hydroxyl and carboxylic acid groups. Meanwhile, Sham et al. [35] demonstrated that ozone surface treatment can improve the dispersion of carbon nanotubes in an epoxy matrix and accelerate the chemical reaction with the epoxy resin. Nevertheless, there have not yet been any studies devoted to research on CFRPs with ozone-modified CB.

The aim of the present research was to study the influence of incorporating ozone-modified CB on the fracture and post-cracking toughness of conventional multi-scale composites. The chemical and morphological changes of ozone-modified CB were investigated. We prepared specimens with different nanofiller content to compare the synergistic effects in the fabricated multi-scale composites. Meanwhile, extending such ozone technology to modify the CB surface could provide a promising approach to the tailoring of desired interfacial properties in multi-scale composites. In addition, this simple method could be beneficial in civil & structural engineering application.

2. Experimental

2.1. Materials

The CFs used in this study were commercial, woven-type (WCF, T-300 grade; Toray Industries Co., Japan). The diglycidyl ether of bisphenol A with an epoxide equivalent weight of 185–190 $g \cdot eq^{-1}$ and a density of ~1.16 $g\,m^{-3}$ at 25 °C was supplied by Kukdo Co., Korea. The curing agent 4,4′-diaminodiphenylmethane (DDM) was purchased from Tokyo Chemical Industry Co., Japan. In addition, the nanofiller CB (N330; particle size: 30–40 nm) was purchased from OCI Co., Korea.

2.2. Ozone surface treatment of CBs

To perform the ozone functionalization of CB, a flow of diluted ozone was controlled from an ozone generator (Ozonetech Co, Lab -Series, Korea) using pure O_2 as the gas source: generator parameters were set to 220 V and 60 Hz to generate ozone from oxygen gas, and ozone was generated at 8 g/h under 0.08 MPa with a gas flow of 0.8 l/min carried out at room temperature for 4 h [36]. The ozone-treated CB were denoted as OCB.

2.3. Fabrication of multi-scale composites

Fig. 1 illustrates the multi-scale OCB/CF/epoxy composite fabrication process. The multi-scale composites were prepared by the following procedure: CB or OCB (1, 3, 5, or 7 wt%) was disperse in acetone, then mixed with epoxy resin and mechanically stirred for 1 h. Thereafter, the mixed OCB/epoxy matrix was heated in a vacuum oven at 120 °C for 50 min to evaporate the acetone. A curing agent (DDM) was then added to the OCB/epoxy mixture, followed by vigorous stirring. When the curing agent was dissolved, the mixture was degassed at 60 °C in a vacuum oven for 30 min to remove the bubbles. Planetary mixing was applied as an efficient method to produce bubble-free composites with uniform nanofiller dispersion at high filler loading. These procedures were repeated twice, and then the resulting mixtures were prepared by continuous impregnation of the CFs using a 3-roll milling machine for manufacturing woven-type prepregs. Following this, the woven-type prepregs were cured by heating to 80 °C for 30 min, then to 120 °C for 20 min, and to 160 °C for 20 min, and finally post-cured at 180 °C for 2 h. We denoted the specimens of CB/CF/epoxy multi-scale composites and OCB/CF/epoxy multi-scale composites as CCE and OCE, respectively.

2.4. Characterization

X-ray diffraction (XRD; PHASER, Bruker Co., Germany) analysis was performed at ambient temperature, and from 5 to 90° (2θ) at a rate of 5° min^{-1}. For Fourier transform-infrared vacuum spectrometry (FT-IR; Vertex 80 V, Bruker Co, USA), the OCB was pressed into pellets with potassium bromide (KBr) and scanned with radiation ranging from 800 to 4000 cm^{-1}. X-ray photoelectron spectroscopy (XPS; K-Alpha, Thermo Co., USA) analysis was performed with monochromated Al Kα radiation (1486.6 eV) as the X-ray source for excitation. The surface morphology of the prepared OCB was investigated using field emission transmission electron microscopy (FE-TEM; JEM-2100F, Jeol Co., UK). High-resolution scanning electron microscopy (HR-SEM; SU8010, Hitachi Tech Co., Japan) was used to observe the morphology of the fractured surfaces of the specimens after spray-coating with platinum.

2.5. Testing of the multi-scale composites

To evaluate the effect of adding OCB on the interfacial properties of the multi-scale composites, their contact angles (CAs) were measured using the sessile drop method on a Ramé-hart CA instrument (Phoenix 300, Ramé-hart Instruments Co., Korea). At least 15 valid tests were carried out and the mean value with a standard deviation below 2° is reported for each composite specimen. CA data using three basic liquids are given in Table S1.

The fracture toughness (K_{IC}) of the composite specimens was measured with a Universal Testing Machine (LR30k, Lloyd Co., UK) using a three-point bending test in compliance with ASTM-E399. K_{IC} for the composite specimens is calculated as [37,38]:

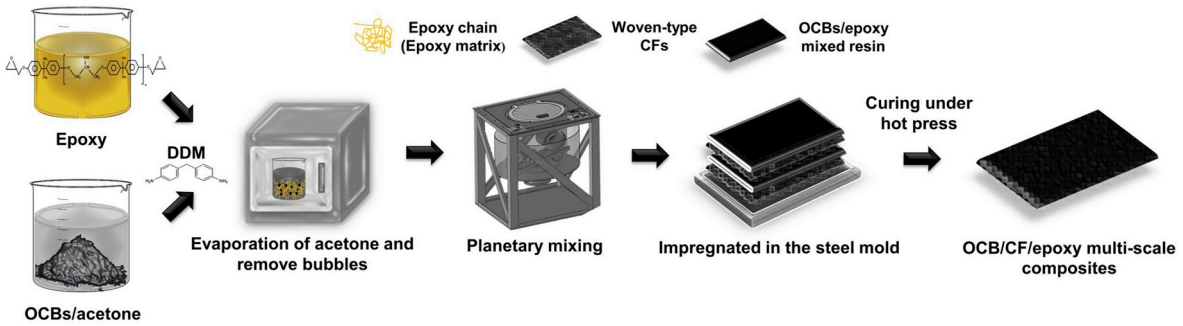

Fig. 1. A schematic representation of the OCB/CF/epoxy multi-scale composite preparation process.

$$K_{IC} = \frac{FL}{bd^{3/2}} \cdot Y \quad (1)$$

where F (N) is the critical load at the crack fracture composite specimen at a distance of L (mm) induced span supports, b and d (mm) are the width and the thickness of the composite specimen, respectively, and

$$Y = \frac{3a/d^{1/2}\left[1.99 - (a/d)(1 - a/d)(2.15 - 3.93a/d + (2.7a^2/d^2)\right]}{2(1 + 2a/d)(1 - a/d)^{3/2}} \quad (2)$$

where a (mm) is the notched length. The notched length was cut using a universal diamond cutting machine (USCM; DYD-302, Daeyeong Co., Korea) to approximately half the depth of the composite specimen.

Short-beam three-point bending tests (ASTM D-2344) were used to evaluate the interlaminar shear strength (ILSS) of the specimens calculated as [39,40]:

$$ILSS = \frac{3F}{4bd}, \quad (3)$$

where the parameters are the same as for K_{IC}.

3. Results and discussion

3.1. Characterization of the OCBs

The XRD patterns of all the CB samples are shown in Fig. 2(a). The diffraction pattern of CB shows two broad peaks corresponding to the (002) and (100) planes of the graphite structure, respectively, implying that it is an amorphous carbon material with small regions of crystallinity due to graphitic crystallites of carbon [41,42]. Moreover, the diffraction pattern of OCB was similar to that of CB, indicating that they had the same crystalline structure and the interplanar spacing of the samples remained the same. Thus, it can be mean that the ozone oxidation process did not change the general crystalline structure of CB.

Fig. 2(b) shows the FT-IR spectra of CBs and OCBs. After ozone treatment for 4 h, new peaks could be observed at 1714.8 and 1378.4 cm^{-1}, which are attributed to the C═O and C–OH stretching vibrations of the carboxyl group (–COOH), respectively [43]. The peaks at 1109.3 and 2921.4 cm^{-1} correspond to the expected C–O and C–H stretching vibrations, respectively, as confirmed by the decrease in the C–C band at 1624.5 cm^{-1} [44,45]. XPS was performed and relative analysis to further confirm the surface composition and chemical status of OCB. The XPS spectra and subsequently detected atomic concentrations of C and O at the CB and OCB surfaces are presented in Fig. 2(c). The O/C ratios of the CB and OCB samples were 0.14 and 0.27 at%, respectively, which confirmed the effectiveness of the ozone process in generating oxygen functional groups on the CB surface.

In addition, the C 1s and O 1s core level peaks were deconvoluted, the results of which are shown in Fig. 3(a) and (b), respectively. Fig. 3(a) shows the C 1s deconvoluted peaks at 284.4, 285.8, and 287.7 eV, corresponding to the C–C, C–O and -O-C═O groups, respectively [46,47], while Fig. 3(b) shows the O 1s deconvoluted peaks at 531.2, 532.5, and 533.8 eV, corresponding to the C═O, -O-C═O, and C–O groups, respectively [46,48]. From the results, the OCB was found to have more carboxylic functional groups on the outer surface compared to the CB. These results are reflected consistently with the above-mentioned FT-IR data.

3.2. Morphology of the OCBs

The difference in surface morphology between the CB and OCB can be observed in Fig. 4(a) and (b). The existence of grooves along the amorphous sidewalls of the OCBs, and ozonization was observed to increase the damage on the OCB surface. This is because the ozone began at the outer layer and progressively removed some of the amorphous sidewalls of the CB through continuous oxidation. In addition, the CB and OCB particle-size distributions were compared via dynamic light scattering; both CB and OCB samples were prepared using ethanol under the same colloidal solution conditions and sonicated for 20 min before characterization. The mean diameter of CB was 172 nm (Fig. 4(c)), which is around 5 times higher than the diameter of the primary particles (30–40 nm). In addition, OCB had a particle-size range of 37–45 nm with an average of 41 nm (Fig. 4(d)). The oxygen molecules adsorbed onto the OCB surface not only decreased the surface tension but also prevented large aggregates by overcoming the van der Waals attraction, thereby maintaining excellent dispersion stability. This is similar to the specified size of the primary particles, which proves that the ozone process was efficient at reducing the aggregation of the CB particles.

3.3. Interfacial properties of the OCE multi-scale composites

The surface free energy of the multi-scale composites is directly related to the fracture behavior, which is directly correlated to practical

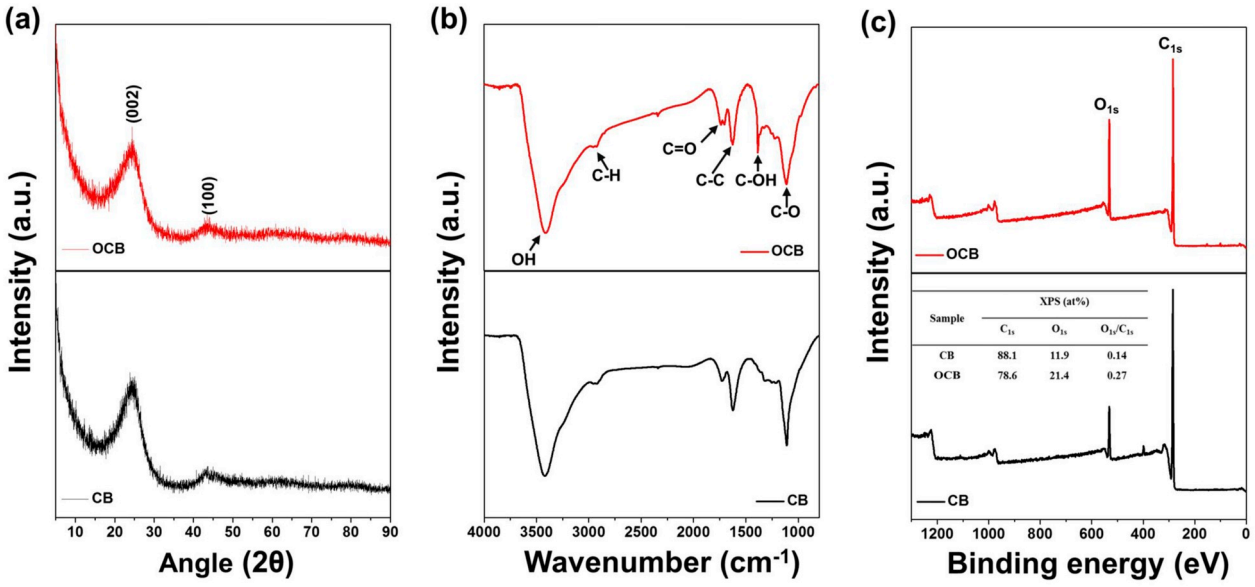

Fig. 2. Characterization of CB and OCB: (a) XRD, (b) FT-IR, and (c) high-resolution XPS spectra.

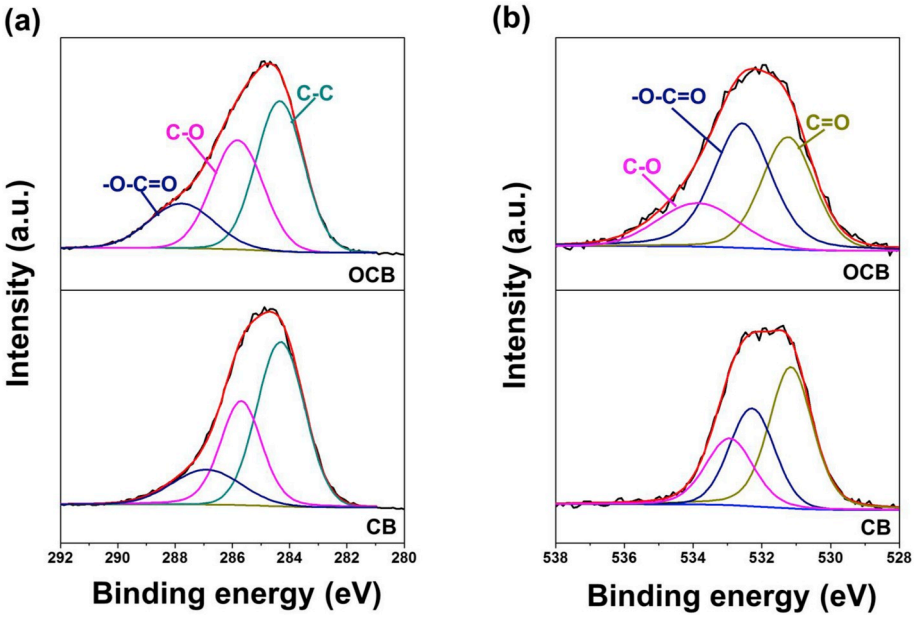

Fig. 3. Characterization of CB and OCB: (a) C 1s and (b) O 1s core level XPS spectra.

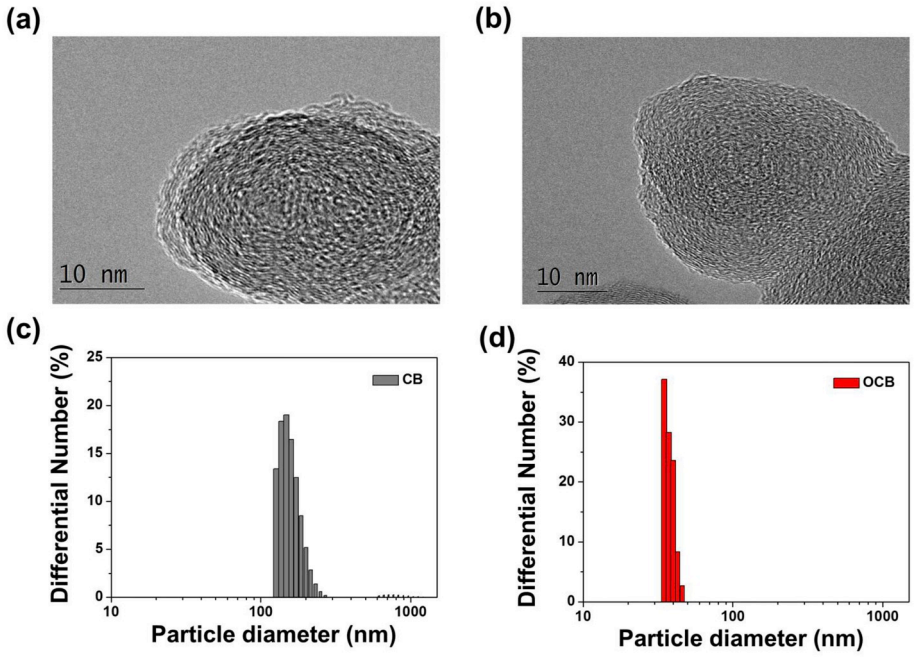

Fig. 4. Surface morphology of CB and OCB: respective FE-TEM images (a), (b) and particle-size distributions (c), (d).

adhesion. According to Owens [49], Kaelble [50], and Fowkes [51], the total surface free energy of a multi-scale composite is often divided into two types of component: specific polar (Keesom's orientational force, Debye-inductive polarization, dipole-induced dipole, hydrogen bonding) and dispersion (London forces). To obtain accurate surface free energy information for the multi-scale composites, these values are calculated based on the CA between the solid and liquid for known surface free energy values:

$$\gamma = \gamma^{L} + \gamma^{SP}, \tag{4}$$

where γ is the surface free energy, γ^{L} is the dispersion components, and γ^{SP} is the specific polar component [51] and

$$\gamma_L(1+\cos\theta) = 2\left(\sqrt{\gamma_S^L \cdot \gamma_L^L} + \sqrt{\gamma_S^{sp} \cdot \gamma_L^{sp}}\right), \tag{5}$$

where θ is the CA of the liquid droplet, subscript L represents the liquid, and subscript S represents a solid [52]. Using three test liquids with Eqs. (4) and (5), one can accurately determine the surface free energy with the following equation [53]:

$$\frac{\gamma_L(1+\cos\theta)}{2\sqrt{\gamma_L^L}} = \sqrt{\gamma_S^{sp}}\left(\frac{\sqrt{\gamma_L^{sp}}}{\sqrt{\gamma_L^L}}\right) + \sqrt{\gamma_S^L}. \tag{6}$$

The surface free energy results for the multi-scale composites calculated from Eq. (6) are reported in Table S2 and shown in Fig. 5(a).

The surface free energy of the OCE multi-scale composites showed an obvious improvement in comparison with that of the CCE multi-scale composites. As presented in Fig. 5(a), the total surface free energy of the CCE multi-scale composites reached roughly from ~44.5 mJ m^{-2} to a maximum of ~48.7 mJ m^{-2}. While, OCE multi-scale composites, as expected, the surface free energy increased much more, ranging from ~45.1 mJ m^{-2} to ~51.3 mJ m^{-2}, indicating that OCB is more compatible with epoxy resin and CFs. Besides, the contact angles decreased up to ~50.7° for distilled water (Fig. S1), indicating that among the interfacial properties of OCE multi-scale composites, the specific polar components on the surface free energy had a greater effect than the dispersion component [54]. In the context of the previously mentioned FT-IR and XPS study results, we found that OCB gave an increase in oxygen functional groups supplied by ozonization, which could have been the main contribution toward the enhanced specific polar components [55,56].

ILSS is one of the best measurements for determining the interfacial strength: it is a critical indicator of the interfacial adhesion of the epoxy matrix and CFs and reveals shear properties that depend on interfacial interactions in the matrix [57–59]. From Fig. 5(b), it is clearly shown that the linear relationship between the surface free energy and the ILSS could improve interfacial adhesion of the multi-scale composites. In this evaluation, the ILSS value of the neat composites showed a low value (21.7 MPa), which is as expected, and the CCE multi-scale composites performed better than the neat composites, but there was still a limit to their effects. Therefore, we suggest that the interactions in the OCE multi-scale composite exert a considerable synergistic effect for enhancing interfacial adhesion. Compared to the CCE-1 (24.6 MPa) and CCE-3 (27.1 MPa) multi-scale composites, ILSS values of for the OCE-1 (26.7 MPa) and OCE-3 (28.9 MPa) multi-scale composites increased by 8.5% and 6.7%, respectively. In particular, the OCE-5 (35.7 MPa) and OCE-7 (30.9 MPa) multi-scale composites showed significant increases of 14.1% and 9.2%, respectively, compared with the CCE-5 (31.3 MPa) and CCE-7 (28.3 MPa) multi-scale composites. The ILSS enhancement of the OCE multi-scale composites could be attributed to the enhanced surface free energy and dispersion between the OCB and the epoxy matrix as well as the increased chemical interlocking caused by the introduction of oxygen groups.

3.4. Fracture toughness of the OCE multi-scale composites

Commonly, the main ability of nanofillers as a reinforcing element in an epoxy matrix is known to enhance K_{IC}, and is an important design factor, particularly for multi-scale composites intended for application in the civil and structural engineering industries [60–64]. The mechanical properties including K_{IC} and load-deflection were studied for both CCE and OCE multi-scale composites to evaluate their effectiveness. Fig. 6(a) shows the K_{IC} results to evaluate the overall mechanical properties of the multi-scale composites. Clearly, all of the OCE multi-scale composites showed significant improvement in K_{IC} compared to the CCE multi-scale composites. Compared with the CCE-1 (61.3 MPa m$^{1/2}$) and CCE-3 (75.8 MPa m$^{1/2}$) multi-scale composites, the K_{IC} values of the OCE-1 (70.5 MPa m$^{1/2}$) and OCE-3 (83.3 MPa m$^{1/2}$) multi-scale composites increased by 15.0% and 9.9%, respectively. In addition, the OCE-5 multi-scale composite (95.7 MPa m$^{1/2}$) increased significantly to 12.5% compared with the CCE-5 multi-scale composite (85.1 MPa m$^{1/2}$). However, when the CB or OCB content reached 7 wt%, a large number of aggregate points were generated inside the multi-scale composites regardless of the type of nanofiller used. These acted as defects and degraded the K_{IC}. It should be highlighted that a higher value of fracture toughness can be obtained by increasing the CB content within a reasonable dosage range.

In addition, the improvements in K_{IC} achieved by the addition of the OCB in this work are compared with the previously reported values for epoxy-based composites containing different types of CBs. The improvements in the values of K_{IC} are normalized based on the type of unmodified epoxy composites (neat) used within the present work and reported in the literature [65–72]. The obtained maximum percentage value was improved compared to other epoxy-based composites reported in the literature, as shown in Table 1, demonstrating the superior efficiency of the composites prepared herein.

We observed the post-cracking toughness in more detail to study the fracture mechanisms acting on the multi-scale composites. Fig. 6(b) shows the load-deflection curves of the neat composites, CCE-5, and OCE-5 multi-scale composites according to K_{IC}. Generally speaking, the fracturing of multi-scale composites can be divided into the crack initiation and propagation stages. As can be seen in Fig. 6(b), *A* is the crack initiation stage (showing a linear response curve for K_{IC}) and *B* denotes the crack propagation stage (showing a non-linear response curve). The post-cracking toughness of the multi-scale composites can be evaluated by the toughness index (*TI*) calculated as

$$TI = \frac{A + B}{A} \tag{7}$$

The neat composites had the smallest *TI* values (1.3) without a non-linear response, and thus showed general brittle fracturing (low toughness), which is as expected. In addition, the *TI* values of the CCE-5 and OCE-5 multi-scale composites were 2.1 and 3.4, respectively, which means that the latter needed more energy during fracturing. These results suggest that additional energy absorption mechanisms were active when the OCB particles were dispersed into the matrix which could increase both K_{IC} and post-cracking toughness of the multi-scale composites.

Fig. 7 depicts the schematic of the fracture mechanisms to directly disclose the fracture and post-crack toughness of the multi-scale composites. As crack opens, processes shown in Fig. 7(a) and (b) can occur, depending on the dispersion and the interfacial adhesion of CBs. For CCE multi-scale composites (Fig. 7(a)), the crack tips can directly contact the fiber surface due to poor dispersion and adhesion in the interface. As a result, the composites can crack easily under a low fracture. On the other hand, in case of an OCE multi-scale composites, a complete rupture of CBs or forming pull-out of the inner CBs can occur. (Fig. 7(b)). Therefore, the achievable fracture and post-crack toughness would have been substantially higher and can be related to dispersion and interfacial

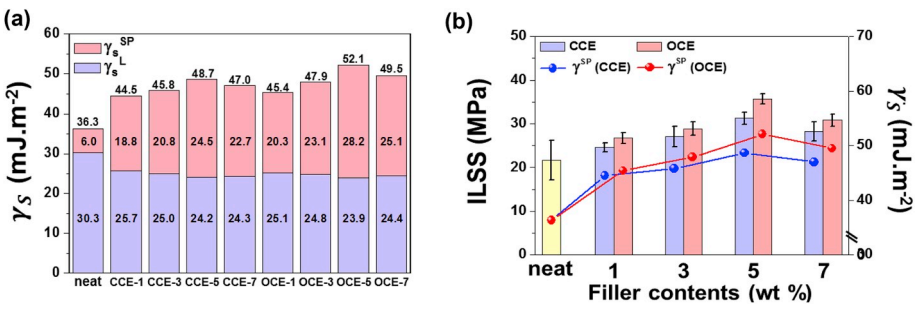

Fig. 5. Interfacial properties of the CCE and OCE multi-scale composites: (a) surface free energy, (b) ILSS.

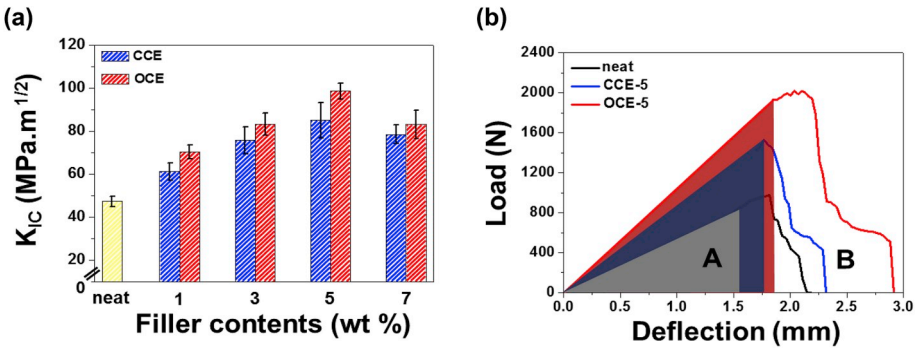

Fig. 6. Mechanical properties of the CCE and OCE multi-scale composites: (a) K_{IC}, (b) load-deflection curves.

Table 1
Comparison of K_{IC} values of the OCE multi-scale composites measured in this work with reported values in the literature.

Refs.	Nanofiller	Filler contents (wt%)	KIC improvement (%)
This work	OCB	5.0	70.8
Gojny et al. [65]	CB	0.1	18.5
Lachman et al. [66]	CB	0.3	5.9
Gojny et al. [67]	CB	0.3	32.3
Kim et al. [68]	CB	3.0	23.0
Zhang et al. [69]	CB/copper chloride hybrid	2.5	14.4
Hsieh et al. [70]	CNT	0.5	42.0
Ma et al. [71]	CB/CNT hybrid	0.2	57.1
Baltzis et al. [72]	CB/CNT hybrid	2.5	61.0

adhesion between CBs and matrix, which raises the dominance of a crack bridging mechanism. Some evidence for these crack bridging mechanisms could be validated on the fractured surfaces presented in the next section.

Fig. 8(a–f) displays SEM images of the fractured surfaces of the neat composites, CCE-5, and OCE-5 multi-scale composites. As shown in Fig. 8(a) and (d), SEM images of the neat composite show a relatively smooth cracked surface of typical brittle fracture mode patterns with regular crack growth. By contrast, the CCE-5 multi-scale composites exhibited a rougher fractured surface (Fig. 8(b) and (e)), and in comparison to the neat composite, showed crack tip arrest and a change in the crack propagation direction, resulting in higher energy absorption capability. However, CCE-5 multi-scale composite's very rough aggregated fractures due to non-homogeneous dispersion of CB, and a closer examination revealed that it was difficult to find pull-out or bridging in the CB-epoxy matrixes. In addition, fractures occurred at low stress due to the low interfacial adhesion between the CB and the matrix, which failed to efficiently support the load of the CFs. On the other hand, the OCE-5 multi-scale composite was not only highly dispersed within the epoxy matrix without large aggregations but also tightly embedded in the epoxy matrix without de-bonding (Fig. 8(c) and (f)). In addition, this provided visual evidence of the strong bonding between the epoxy matrix and the OCB that resulted in minimal pull-out of the OCB. This fracture pattern supports the findings of the highest levels of K_{IC} and post-cracking toughness being associated with the best dispersibility and interfacial adhesion.

4. Conclusions

In this study, ozone-functionalized CB nanofillers were utilized for use as reinforcement in multi-scale composites. After ozone

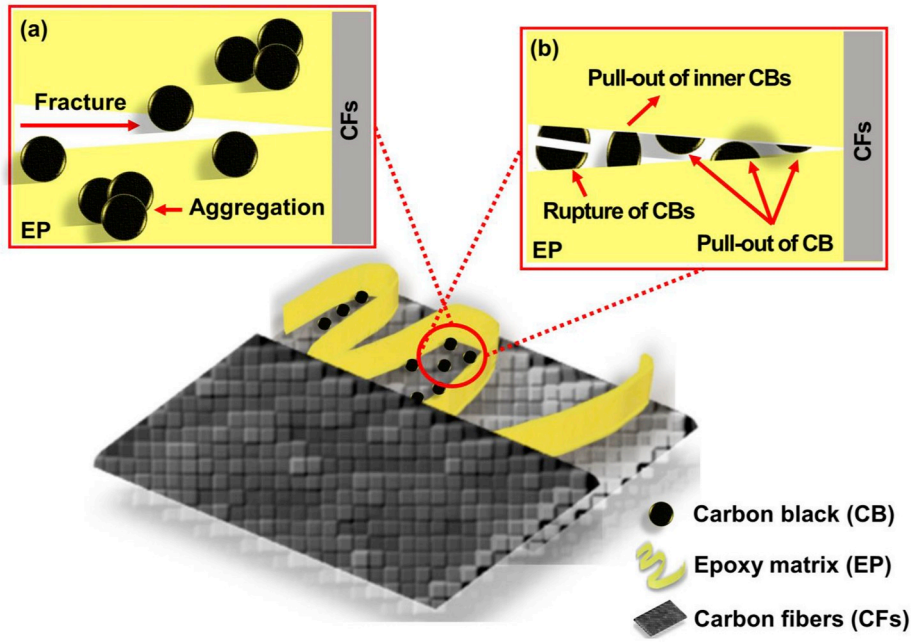

Fig. 7. Schematic description of crack bridging mechanism: (a) CCE multi-scale composites, (b) OCE multi-scale composites.

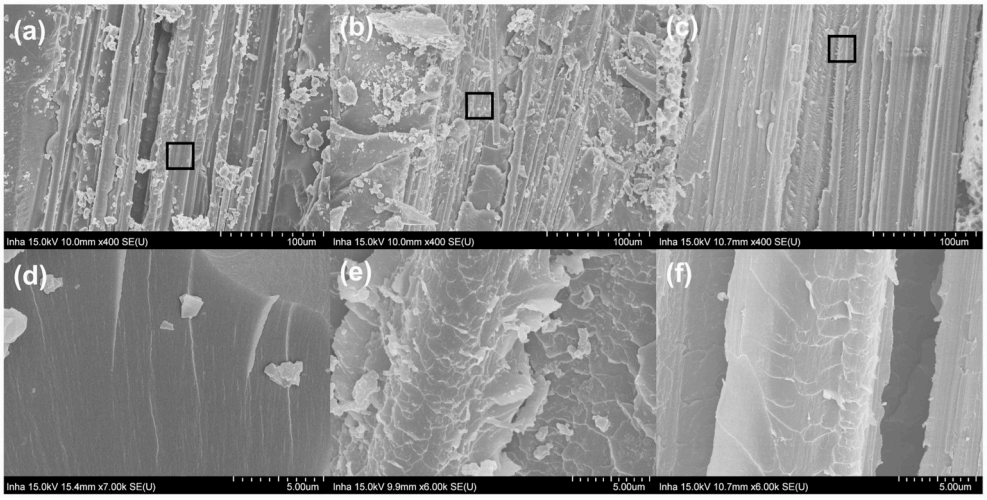

Fig. 8. Fracture surfaces of CCE and OCE multi-scale composites: (a) neat, (b) CCE-5, and (c) OCE-5. (d), (e), and (f) are the magnified fractured surface of the closed regions in (a), (b), and (c), respectively.

functionalization, the introduction of hydroxyl and carboxyl functionalities on the CB surface significantly improved dispersibility due to improved chemical interactions. In addition, they were incorporated within the epoxy matrix to improve the interfacial adhesion within, which consequently improved the interlaminar shear strength of the multi-scale composites. For all of the multi-scale composites developed, the ozone-functionalized CB content was found to be optimal at 5 wt%, which was effective in improving fracture and post-cracking toughness under the same load. However, the degradation of fracture toughness with increasing CB content could be associated with particle aggregation due to the strong van der Waals forces that usually develop between CB particles. As such, our efforts could promote the conversion of multi-scale composites into high-performance materials and offer more rational guidance and fundamental understanding toward realizing the theoretical limits of interfacial and mechanical properties.

Competing Interests

The authors declare that they have no competing interests.

Acknowledgments

This research was supported by Korea Evaluation institute of Industrial Technology (KEIT) through the Carbon Cluster Construction project(10083586, Development of petroleum based graphite fibers with ultra-high thermal conductivity) funded by the Ministry of Trade, Industry and Energy (MOTIE, Korea) and the Commercialization Promotion Agency for R and D Outcomes (COMPA) funded by the Ministry of Science and ICT(MSIT)(2018_RND_002_0064, Development of 800 mAh/g pitch carbon coating materials).

Appendix A. Supplementary data

Supplementary data to this article can be found online at https://doi.org/10.1016/j.compositesb.2019.107379.

References

[1] Yu K, Shi Q, Dunn ML, Wang T, Qi HJ. Carbon fiber reinforced thermoset composite with near 100% recyclability. Adv Funct Mater 2016;26(33):6098–106.
[2] Forintos N, Czigany T. Multifunctional application of carbon fiber reinforced polymer composites: electrical properties of the reinforcing carbon fibers–A short review. Compos B Eng 2019;162(1):331–43.
[3] Godara A, Mezzo L, Luizi F, Warrier A, Lomov SV, Van Vuure AW, Verpoest I. Influence of carbon nanotube reinforcement on the processing and the mechanical behaviour of carbon fiber/epoxy composites. Carbon 2009;47(12):2914–23.
[4] Zheng N, Liu HY, Gao J, Mai YW. Synergetic improvement of interlaminar fracture energy in carbon fiber/epoxy composites with nylon nanofiber/polycaprolactone blend interleaves. Compos B Eng 2019;171:320–8.
[5] Pathak AK, Borah M, Gupta A, Yokozeki T, Dhakate SR. Improved mechanical properties of carbon fiber/graphene oxide-epoxy hybrid composites. Compos Sci Technol 2016;135:28–38.
[6] Shahabi R, Narmashiri K. Effects of deficiency location on CFRP strengthening of steel CHS short columns. Steel Compos Struct 2018;28(3):267–78.
[7] Zhang RL, Gao B, Du WT, Zhang J, Cui HZ, Liu L, Li FH. Enhanced mechanical properties of multiscale carbon fiber/epoxy composites by fiber surface treatment with graphene oxide/polyhedral oligomeric silsesquioxane. Compos A Appl Sci Manuf 2016;84:455–63.
[8] Abidin MSZ, Herceg T, Greenhalgh ES, Shaffer M, Bismarck A. Enhanced fracture toughness of hierarchical carbon nanotube reinforced carbon fibre epoxy composites with engineered matrix microstructure. Compos Sci Technol 2019;170:85–92.
[9] Quan D, Urdániz JL, Ivanković A. Enhancing mode-I and mode-II fracture toughness of epoxy and carbon fibre reinforced epoxy composites using multi-walled carbon nanotubes. Mater Des 2018;143:81–92.
[10] Batista MDR, Drzal LT. Carbon fiber/epoxy matrix composite interphases modified with cellulose nanocrystals. Compos Sci Technol 2018;164:274–81.
[11] Carolan D, Ivankovic A, Kinloch AJ, Sprenger S, Taylor AC. Toughened carbon fibre-reinforced polymer composites with nanoparticle-modified epoxy matrices. J Mater Sci 2017;52(3):1767–88.
[12] Tsai SN, Carolan D, Sprenger S, Taylor AC. Fracture and fatigue behaviour of carbon fibre composites with nanoparticle-sized fibres. Compos Struct 2019;217:143–9.
[13] Du X, Zhou H, Sun W, Liu HY, Zhou G, Zhou H, Mai YW. Graphene/epoxy interleaves for delamination toughening and monitoring of crack damage in carbon fibre/epoxy composite laminates. Compos Sci Technol 2017;140:123–33.
[14] Adak NC, Chhetri S, Kuila T, Murmu NC, Samanta P, Lee JH. Effects of hydrazine reduced graphene oxide on the inter-laminar fracture toughness of woven carbon fiber/epoxy composite. Compos B Eng 2018;149:22–30.
[15] Ning H, Li J, Hu N, Yan C, Liu Y, Wu L, Zhang J. Interlaminar mechanical properties of carbon fiber reinforced plastic laminates modified with graphene oxide interleaf. Carbon 2015;91:224–33.
[16] Shin HC, Cho WI, Jang H. Electrochemical properties of carbon-coated $LiFePO_4$ cathode using graphite, carbon black, and acetylene black. Electrochim Acta 2006;52(4):1472–6.
[17] Dong J, Jia C, Wang M, Fang X, Wei H, Xie H, Huang Y. Improved mechanical properties of carbon fiber-reinforced epoxy composites by growing carbon black on carbon fiber surface. Compos Sci Technol 2017;149:75–80.
[18] Huynh MTT, Cho HB, Suzuki T, Suematsu H, Nguyen ST, Niihara K, Nakayama T. Electrical property enhancement by controlled percolation structure of carbon black in polymer-based nanocomposites via nanosecond pulsed electric field. Compos Sci Technol 2018;154:165–74.
[19] White AH, Germer LH. The structure of black carbon. J Chem Phys 1941;9(7):492–7.
[20] Papirer E, Dentzer J, Li S, Donnet JB. Surface groups on nitric acid oxidized carbon black samples determined by chemical and thermodesorption analyses. Carbon 1991;29(1):69–72.
[21] Cho W, Lee SH, Ju WS, Baek Y, Lee JK. Conversion of natural gas to hydrogen and carbon black by plasma and application of plasma carbon black. Catal Today 2004;98(4):633–8.
[22] Papirer E, Dentzer J, Li S, Donnet JB. Surface groups on nitric acid oxidized carbon black samples determined by chemical and thermodesorption analyses. Carbon 1991;29(1):69–72.

[23] Cho W, Lee SH, Ju WS, Baek Y, Lee JK. Conversion of natural gas to hydrogen and carbon black by plasma and application of plasma carbon black. Catal Today 2004;98(4):633–8.
[24] Loos MR, Yang J, Feke DL, Manas-Zloczower I. Effect of block-copolymer dispersants on properties of carbon nanotube/epoxy systems. Compos Sci Technol 2012;72(4):482–8.
[25] Ghasemi-Kahrizsangi A, Shariatpanahi H, Neshati J, Akbarinezhad E. Degradation of modified carbon black/epoxy nanocomposite coatings under ultraviolet exposure. Appl Surf Sci 2015;353:530–9.
[26] Zhang Q, Rastogi S, Chen D, Lippits D, Lemstra PJ. Low percolation threshold in single-walled carbon nanotube/high density polyethylene composites prepared by melt processing technique. Carbon 2006;44(4):778–85.
[27] Phua JL, Teh PL, Ghani SA, Yeoh CK. Influence of thermoplastic spacer on the mechanical, electrical, and thermal properties of carbon black filled epoxy adhesives. Polym Adv Technol 2017;28(3):345–52.
[28] Li M, Boggs M, Beebe TP, Huang CP. Oxidation of single-walled carbon nanotubes in dilute aqueous solutions by ozone as affected by ultrasound. Carbon 2008;46(3):466–75.
[29] Li FN, Akhvlediani R, Kuntumalla MK, Hoffman A. Oxygen bonding configurations and defects on differently oxidized diamond surfaces studied by high resolution electron energy loss spectroscopy and X-ray photoelectron spectroscopy measurements. Appl Surf Sci 2019;465:313–9.
[30] Efimenko K, Wallace WE, Genzer J. Surface modification of Sylgard-184 poly (dimethyl siloxane) networks by ultraviolet and ultraviolet/ozone treatment. J Colloid Interface Sci 2002;254(2):306–15.
[31] Fu X, Lu W, Chung DDL. Ozone treatment of carbon fiber for reinforcing cement. Carbon 1998;36(9):1337–45.
[32] Chu H, Hao W, Cheng Z, Huang Y, Wang S, Shang J, Zhou W. Black carbon particles and ozone-oxidized black carbon particles induced lung damage in mice through an interleukin-33 dependent pathway. Sci Total Environ 2018;644:217–28.
[33] Chiang HL, Huang CP, Chiang PC. The surface characteristics of activated carbon as affected by ozone and alkaline treatment. Chemosphere 2002;47(3):257–65.
[34] Arnault JC. X-ray photoemission spectroscopy applied to nanodiamonds: from surface chemistry to in situ reactivity. Diam Relat Mat 2018;84:157–68.
[35] Sham ML, Kim JK. Surface functionalities of multi-wall carbon nanotubes after UV/Ozone and TETA treatments. Carbon 2006;44(4):768–77.
[36] Tang LC, Zhang H, Han JH, Wu XP, Zhang Z. Fracture mechanisms of epoxy filled with ozone functionalized multi-wall carbon nanotubes. Compos Sci Technol 2011;72(1):7–13.
[37] Dong W, Liu HC, Park SJ, Jin FL. Fracture toughness improvement of epoxy resins with short carbon fibers. J Ind Eng Chem 2014;20(4):1220–2.
[38] Galpaya D, Wang M, George G, Motta N, Waclawik E, Yan C. Preparation of graphene oxide/epoxy nanocomposites with significantly improved mechanical properties. J Appl Phys 2014;116(5):053518.
[39] Ryu SK, Park BJ, Park SJ. XPS analysis of carbon fiber surfaces-anodized and interfacial effects in fiber–epoxy composites. J Colloid Interface Sci 1999;215(1):167–9.
[40] Alzeebaree R, Gulsan ME, Nis A, Mohammedameen A, Cevik A. Performance of FRP confined and unconfined geopolymer concrete exposed to sulfate attacks. Steel Compos Struct 2018;29(2):201–18.
[41] Hu E, Hu X, Liu T, Fang L, Dearn KD, Xu H. The role of soot particles in the tribological behavior of engine lubricating oils. Wear 2013;304(1–2):152–61.
[42] Asokan V, Kosinski P, Skodvin T, Myrseth V. Characterization of carbon black modified by maleic acid. Front Mater Sci 2013;7(3):302–7.
[43] Zappielo CD, Nanicuacua DM, dos Santos WN, da Silva DL, Dall'Antônia LH, Oliveira FMD, Tarley CR. Solid phase extraction to on-line preconcentrate trace cadmium using chemically modified nano-carbon black with 3-mercaptopropyltrimethoxysilane. J Braz Chem Soc 2016;27(10):1715–26.
[44] Cheng CH, Lehmann J, Thies JE, Burton SD, Engelhard MH. Oxidation of black carbon by biotic and abiotic processes. Org Geochem 2006;37(11):1477–88.
[45] Sutherland I, Sheng E, Bradley RH, Freakley PK. Effects of ozone oxidation on carbon black surfaces. J Mater Sci 1996;31(21):5651–5.
[46] Müller JO, Su DS, Wild U, Schlögl R. Bulk and surface structural investigations of diesel engine soot and carbon black. Phys Chem Chem Phys 2007;9(30):4018–25.
[47] Shao Y, Yin G, Zhang J, Gao Y. Comparative investigation of the resistance to electrochemical oxidation of carbon black and carbon nanotubes in aqueous sulfuric acid solution. Electrochim Acta 2006;51(26):5853–7.
[48] Strzemiecka B, Voelkel A, Donate-Robles J, Martín-Martínez JM. Assessment of the surface chemistry of carbon blacks by TGA-MS, XPS and inverse gas chromatography using statistical chemometric analysis. Appl Surf Sci 2014;316:315–23.
[49] Owens DK, Wendt RC. Estimation of the surface free energy of polymers. J Appl Polym Sci 1969;13(8):1741–7.
[50] Kaelble DH. Dispersion-polar surface tension properties of organic solids. J Adhes 1970;2(2):66–81.
[51] Fowkes FM. Determination of interfacial tensions, contact angles, and dispersion forces in surfaces by assuming additivity of intermolecular interactions in surfaces. J Phys Chem 1962;66(2). 382-382.
[52] Park SJ, Brendle M. London dispersive component of the surface free energy and surface enthalpy. J Colloid Interface Sci 1997;188(2):336–9.
[53] Park SJ, Donnet JB. Anodic surface treatment on carbon fibers: determination of acid-base interaction parameter between two unidentical solid surfaces in a composite system. J Colloid Interface Sci 1998;206(1):29–32.
[54] Kang WS, Rhee KY, Park SJ. Influence of surface energetics of graphene oxide on fracture toughness of epoxy nanocomposites. Compos B Eng 2017;114:175–83.
[55] Kim KS, Lee KH, Cho K, Park CE. Surface modification of polysulfone ultrafiltration membrane by oxygen plasma treatment. J Membr Sci 2002;199(1–2):135–45.
[56] Xing L, Liu L, Huang Y, Jiang D, Jiang B, He J. Enhanced interfacial properties of domestic aramid fiber-12 via high energy gamma ray irradiation. Compos B Eng 2015;69:50–7.
[57] Shi XH, Xu YJ, Long JW, Zhao Q, Ding XM, Chen L, Wang YZ. Layer-by-layer assembled flame-retardant architecture toward high-performance carbon fiber composite. Chem Eng J 2018;353:550–8.
[58] Zhao X, Zhang L, Alonso JP, Delgado S, Martínez-Miranda MR, Wang DY. Influence of phenylphosphonic amide on rheological, mechanical and flammable properties of carbon fiber/RTM6 composites. Compos B Eng 2018;149:74–81.
[59] Lakshmipathi J, Vasudevan R. Dynamic characterization of a CNT reinforced hybrid uniform and non-uniform composite plates. Steel Compos Struct 2019;30(1):31–46.
[60] Kim SH, Heo YJ, Park M, Min BG, Rhee KY, Park SJ. Effect of hydrophilic graphite flake on thermal conductivity and fracture toughness of basalt fibers/epoxy composites. Compos B Eng 2018;153:9–16.
[61] Ladani RB, Wu S, Kinloch AJ, Ghorbani K, Zhang J, Mouritz AP, Wang CH. Improving the toughness and electrical conductivity of epoxy nanocomposites by using aligned carbon nanofibres. Compos Sci Technol 2015;117:146–58.
[62] Wu S, Ladani RB, Zhang J, Bafekrpour E, Ghorbani K, Mouritz AP, Wang CH. Aligning multilayer graphene flakes with an external electric field to improve multifunctional properties of epoxy nanocomposites. Carbon 2015;94:607–18.
[63] Kim SH, Heo YJ, Park SJ. Ozonization of SWCNTs on thermal/mechanical properties of basalt fiber-reinforced composites. Steel Compos Struct 2019;31(5):517–27.
[64] Ravindran AR, Ladani RB, Wu S, Kinloch AJ, Wang CH, Mouritz AP. Multi-scale toughening of epoxy composites via electric field alignment of carbon nanofibres and short carbon fibres. Compos Sci Technol 2018;167:115–25.
[65] Gojny FH, Wichmann MHG, Köpke U, Fiedler B, Schulte K. Carbon nanotube-reinforced epoxy-composites: enhanced stiffness and fracture toughness at low nanotube content. Compos Sci Technol 2004;64(15):2363–71.
[66] Lachman N, Wagner HD. Correlation between interfacial molecular structure and mechanics in CNT/epoxy nano-composites. Compos A Appl Sci Manuf 2010;41(9):1093–8.
[67] Gojny FH, Wichmann MH, Fiedler B, Schulte K. Influence of different carbon nanotubes on the mechanical properties of epoxy matrix composites–a comparative study. Compos Sci Technol 2005;65(15–16):2300–13.
[68] Kim BC, Park SW. Fracture toughness of the nano-particle reinforced epoxy composite. Compos Struct 2008;86(1–3):69–77.
[69] Zhang D, Ye L, Deng S, Zhang J, Tang Y, Chen Y. CF/EP composite laminates with carbon black and copper chloride for improved electrical conductivity and interlaminar fracture toughness. Compos Sci Technol 2012;72(3):412–20.
[70] Hsieh TH, Kinloch AJ, Taylor AC, Kinloch IA. The effect of carbon nanotubes on the fracture toughness and fatigue performance of a thermosetting epoxy polymer. J Mater Sci 2011;46(23):7525.
[71] Ma PC, Liu MY, Zhang H, Wang SQ, Wang R, Wang K, Kim JK. Enhanced electrical conductivity of nanocomposites containing hybrid fillers of carbon nanotubes and carbon black. ACS Appl Mater Interfaces 2009;1(5):1090–6.
[72] Baltzis D, Bekas DG, Tzachristas G, Parlamas A, Karabela M, Zafeiropoulos NE, Paipetis AS. Multi-scaled carbon reinforcements in ternary epoxy composite materials: dispersion and electrical impedance study. Compos Sci Technol 2017;153:7–17.